Journal of Cerebral Blood Flow & Metabolism (2011) 31, 1403–1411

www.jcbfm.com

Arterial spin labeling and dynamic susceptibility contrast CBF MRI in postischemic hyperperfusion, hypercapnia, and after mannitol injection

Yoji Tanaka[1,2], Tsukasa Nagaoka[1], Govind Nair[1], Kikuo Ohno[2] and Timothy Q Duong[3,4]

[1]*Yerkes Imaging Center, Yerkes National Primate Research Center, Emory University, Atlanta, Georgia, USA;* [2]*Department of Neurosurgery, Tokyo Medical and Dental University, Tokyo, Japan;* [3]*Departments of Ophthalmology, Radiology, and Physiology, Research Imaging Institute, University of Texas Health Science Center at San Antonio, San Antonio, Texas, USA;* [4]*Department of Veterans Affairs, South Texas Veterans Health Care System, San Antonio, Texas, USA*

Arterial spin labeling (ASL) and dynamic susceptibility contrast (DSC) magnetic resonance imaging (MRI) are widely used to image cerebral blood flow (CBF) in stroke. This study examined how changes in tissue spin-lattice relaxation-time constant (T_1), blood–brain barrier (BBB) permeability, and transit time affect CBF quantification by ASL and DSC in postischemic hyperperfusion in the same animals. In Group I (n=6), embolic stroke rats imaged 48 hours after stroke showed regional hyperperfusion. In normal pixels, ASL- and DSC-CBF linearly correlated pixel-by-pixel. In hyperperfusion pixels, ASL-CBF was significantly higher than DSC-CBF pixel-by-pixel (by 25%). T_1 increased from 1.76 ± 0.14 seconds in normal pixels to 1.93 ± 0.17 seconds in hyperperfusion pixels. Arterial transit time decreased from 300 milliseconds in normal pixels to 200 milliseconds in hyperperfusion pixels. ΔR_2^* profiles showed contrast-agent leakages in the hyperperfusion regions. In Group II (n=3) in which hypercapnic inhalation was used to increase CBF without BBB disruption, CBF increased overall but ASL- and DSC-CBF remained linearly correlated. In Group III (n=3) in which mannitol was used to break the BBB, ASL-CBF was significantly higher than DSC-CBF. We concluded that in normal tissue, ASL and DSC provide comparable quantitative CBF, whereas in postischemic hyperperfusion, ASL-CBF and DSC-CBF differed significantly because ischemia-induced changes in T_1 and BBB permeability affected the two methods differently.
Journal of Cerebral Blood Flow & Metabolism (2011) **31,** 1403–1411; doi:10.1038/jcbfm.2010.228; published online 22 December 2010

Keywords: arterial spin labeling; arterial transit time; cerebral blood flow; dynamic susceptibility contrast; permeability; spin-lattice relaxation-time constant

Introduction

Accurate quantification of cerebral blood flow (CBF) could lead to improved clinical diagnosis of many neurologic diseases, including stroke. Magnetic resonance imaging (MRI) of CBF offers many advantages compared with other techniques. Cerebral blood flow is widely measured using arterial spin labeling (ASL) or dynamic susceptibility contrast (DSC) technique based on MRI. Arterial spin labeling is a completely noninvasive method and repeated measurements can be made to increase signal-to-noise ratio and spatial resolution because of the favorable short half-life (spin-lattice relaxation-time constant T_1) of endogenous water (Chalela *et al*, 2000; Detre *et al*, 1992; Kim, 1995; Williams *et al*, 1992). Dynamic susceptibility contrast imaging is time efficient and provides various cerebral hemodynamic parameters, such as CBF, cerebral blood volume, and arterial transit time (Ostergaard *et al*, 1996*b*; Smith *et al*, 2000). Absolute quantification of both ASL- and DSC-CBF methods, however, remains an active area of research. Specifically, the effects of spin-lattice relaxation-time constant, arterial transit time, and blood–brain barrier (BBB) permeability on ASL- and DSC-CBF quantification (Alsop and Detre, 1996; Donahue *et al*, 2000; Ostergaard *et al*, 1996*b*; Parkes and Tofts, 2002; Smith *et al*, 2000; Williams *et al*, 1992; Wu *et al*, 2003*a*; Zaharchuk *et al*, 2010), especially under perturbed conditions, remain poorly understood.

Postischemic hyperperfusion is a common phenomenon associated with cerebral infarction. Early

Correspondence: Dr TQ Duong, Research Imaging Institute, UTHSCSA, 8403 Floyd Curl Drive, San Antonio, TX 78229, USA. E-mail: duongt@uthscsa.edu
Received 19 September 2010; revised 25 October 2010; accepted 21 November 2010; published online 22 December 2010

postischemic hyperperfusion has been reported to be both beneficial (i.e., prevent infarct growth) and harmful (i.e., aggravate edema and hemorrhage, and neuronal damage from reperfusion injury) (Pan *et al*, 2007; Schaller and Graf, 2004). Postischemic hyperperfusion in the subacute stage (48 hours after onset) has often been associated with tissue necrosis. The mechanisms of hyperperfusion are unknown and likely multifactorial (Marchal *et al*, 1999). In addition to many CBF regulating factors that are released during ischemia (Macfarlane *et al*, 1991), ischemia also affects tissue T_1, T_2, delayed arterial transit time, vascular resistance, and BBB disruption (Schaller and Graf, 2004) that could affect ASL- and DSC-CBF quantification. To improve understanding of postischemic hyperperfusion, it may be helpful to accurately measure CBF and understand how various biophysical and physiological parameters affect CBF under perturbed conditions.

The goal of this study was to examine the underlying factors that might have contributed to the differences in ASL- and DSC-CBF measurements in postischemic hyperperfusion at acute (2 hours after ischemia) and subacute (48 hours) phase in the same animals. Specifically, we examined how changes in tissue spin-lattice relaxation-time constant, BBB permeability, and arterial transit time affect ASL- and DSC-CBF quantification in three experimental groups: (1) postischemic hyperperfusion in embolic stroke rats, (2) normal animals breathing 5% CO_2 to increase CBF by dilating vessels without BBB disruption, and (3) normal animals injected with mannitol to modulate BBB permeability by osmotic shock (Rapoport, 2000). Arterial spin labeling CBF at different postlabeling delays (PLDs) and DSC-CBF, spin-lattice relaxation-rate constant and magnetic resonance angiography (MRA) were measured in the same animals.

Materials and methods

Animal Preparation

Experiments were performed in accordance with a protocol approved by the institutional animal care and use committee. Male Sprague-Dawley rats (Charles River, Wilmington, MA, USA) weighing 200 to 250 g were anesthetized with 1.5% isoflurane. They were orally intubated and mechanically ventilated. Rectal temperature was maintained at 37°C to 38°C throughout the experiment using an auto-feedback warm water pad. The left femoral artery and vein were cannulated with PE-50 catheters for continuous monitoring of blood pressure and drug injection, respectively. The inspired O_2 and expired CO_2 concentrations were monitored continuously, and tidal volume was adjusted to maintain an end-tidal CO_2 of 35 to 45 mm Hg throughout the experiments. Blood pressure, heart rate, and respiration rate were also maintained within normal physiologic ranges.

Three groups of experiments were performed as outlined in Figure 1. Magnetic resonance imaging consisted of ASL-CBF, DSC-CBF, and T_1 measurements. Time-of-flight (2D) MRA measurements were made in the stroke group to confirm recanalization.

Stroke group ($n = 6$): Embolic stroke was induced following procedures reported previously (Tanaka *et al*, 2007). Briefly, the right carotid artery was exposed. Retrograde cannulation was performed on the right external carotid artery with a PE-50 tubing, with its tip placed close to the carotid bifurcation for delivering clots toward the brain. Blood clots, obtained 24 hours before the stroke induction from the same animal, were injected to induce embolic

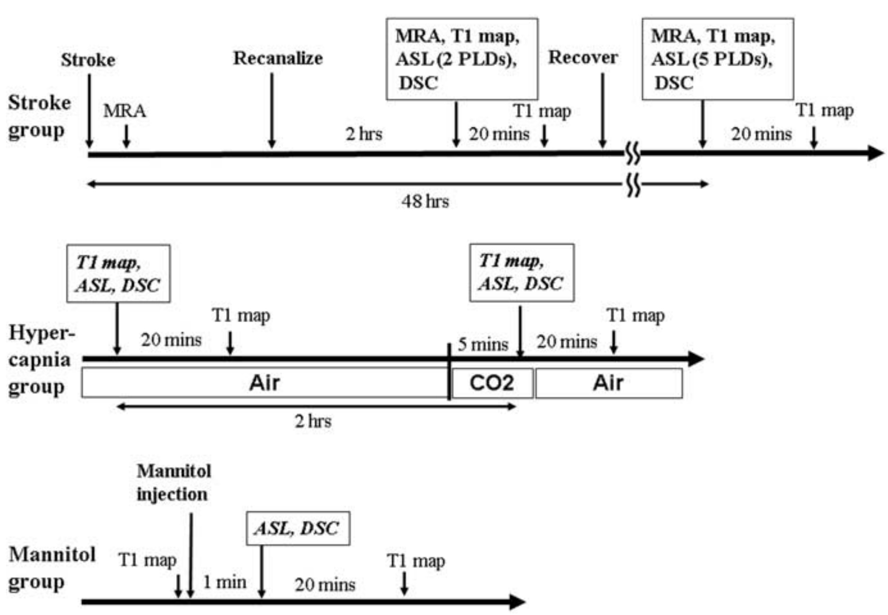

Figure 1 Schematic drawings of the magnetic resonance imaging (MRI) protocols used in the three experimental groups.

stroke. One hour after clot embolism, animals received intravenous infusion of recombinant tissue plasminogen activator (10 mg/kg; Genetech, South San Francisco, CA, USA) dissolved in 2 mL of distilled water. Ten percent of the solution was given as a bolus, and the rest was given as a constant infusion over 1 hour. Magnetic resonance imaging was performed and the animals were allowed to recover and returned to standard animal housing. The animals were anesthetized again after 48 hours for a second set of MRI scans, and then euthanized. Note that these six rats herein (out of the seven rats) showed partial or total recanalization as confirmed by ASL-CBF map and MRA, and substantial CBF recovery within 1 hour after recombinant tissue plasminogen activator administration. All six rats survived for 48 hours after stroke.

Hypercapnia group ($n = 3$): Cerebral blood flow measurements were performed on normal rats associated with hypercapnic inhalation, which increased CBF without BBB disruption. As CO_2 inhalation affected global CBF, normalization with respect to contralateral hemisphere was not possible, and thus two sets of CBF measurement were made in the same animals. First, ASL-CBF and DSC-CBF measurements were made during room air. To avoid gadopentetate dimeglumine (Gd-DTPA) effect of the first DSC measurement on the second ASL measurement, we waited 2 hours before initiating the second set of CBF measurements during hypercapnic inhalation (5% CO_2, 21% O_2, and balance N_2). The 2-hour wait time was used to avoid Gd-DTPA effects on ASL contrast and was experimentally determined to be sufficient by monitoring ASL contrast returning to that of baseline (air).

Mannitol group (Group III, $n = 3$): Normal rats were anesthetized and their right carotid artery was exposed. Retrograde cannulation was performed on the right external carotid artery with a PE-50 tubing, with its tip placed close to the carotid bifurcation for delivering mannitol toward the brain. T_1 MRI measurements were made. Mannitol (0.25 mL 25% mannitol dissolved in phosphate buffer at the rate of 0.5 mL/min) was then infused. Cerebral blood flow measurements were made starting 1 minute after mannitol injection. T_1 MRI measurements were made again (about 20 minutes after mannitol injection). Mannitol was expected to break the BBB for 30 to 45 minutes (Duong *et al*, 2000).

Magnetic Resonance Imaging Measurements

All MRI was performed on a Bruker 7-T/30-cm scanner with a 40-G/cm gradient insert (ID = 12 cm, 120 milliseconds rise time) (Billerica, MA, USA). The rats were placed into a stereotaxic headset and then onto an animal holder, which consisted of an actively decoupled surface coil (2.3 cm ID) for brain imaging and a butterfly neck coil for ASL (Duong *et al*, 2000; Shen *et al*, 2003, 2004).

Arterial spin labeling CBF images were acquired using gradient-echo echo-planar imaging with matrix = 64×64, field of view = $2.56 \times 2.56\,\text{cm}^2$, spectral width = 200 kHz, repetition time (TR) = 2.8 seconds (90° flip angle), echo time (TE) = 13.48 milliseconds, three 1.5 mm slices (Shen *et al*, 2003, 2004). Labeling duration was 2.3 seconds. Post-labeling delays of 100, 200, 300, 400, and 500 milliseconds were used in stroke group, and 100 milliseconds in hypercapnia and mannitol groups. Paired images were acquired alternately one with and the other without, ASL preparation. Sixty pairs of images (total time ~5 minutes) were acquired for signal averaging.

Dynamic susceptibility contrast CBF measurements were performed using identical parameters as the ASL except with TR = 200 milliseconds (90° flip angle) and TE = 13.46 milliseconds. A total of 200 scans were obtained continuously in 40 seconds. A 0.2 mg/kg bolus of Gd-DTPA was injected 15 seconds from the start of the scan via the left femoral vein. Dynamic susceptibility contrast CBF measurements were made after ASL-CBF measurement to avoid contrast agent confounding ASL-CBF measurements.

Two sets of T_1 maps were obtained to investigate the effect of BBB disruption in all groups, one before DSC-CBF (pre-Gd-DTPA) and another 20 minutes after (post-Gd-DTPA). T_1 map was calculated using multiple inversion-recovery echo-planar imaging sequence acquired with identical field of view and imaging matrix as the ASL and DSC images, but with TR = 12,000 milliseconds, TE = 31 milliseconds, and number of average = 1. Twenty-four inversion delays, ranging from 25 to 4,625 milliseconds in 200 milliseconds increments, were used for the calculation.

2D time-of-flight angiography was acquired to identify large vessels using TR = 20 milliseconds, flip angle = 80°, TE = 6.3 milliseconds, slice thickness = 0.9 mm, field of view = $2.56 \times 2.56\,\text{cm}^2$, matrix = 128×128, 20 slices, and 4 averages.

Data Analysis

Data analysis was performed using codes written in Matlab (MathWorks, Natick, MA, USA) software. All data were reported as mean ± s.d. Unpaired *t*-test was used to compare among groups and between normal pixels and hyperperfusion pixels and paired *t*-test was used for the rest of the analysis with $P < 0.05$ considered to be statistically significant.

Quantitative ASL-CBF (mL/100 g per minute) was calculated pixel-by-pixel using: $\text{CBF} = \lambda/T_1(S_C - S_L)/(S_L + (2\alpha - 1)S_C)$, where S_C and S_L are the signal intensities of the control and labeled images, respectively; λ, the water brain–blood partition coefficient, was taken to be 0.9 (Herscovitch and Raichle, 1985); T_1 was the water spin-lattice relaxation time of tissue; and α, the ASL efficiency (Williams *et al*, 1992), was measured to be 0.75 (Shen *et al*, 2003, 2004). The signal difference between the control image and labeled image ($\Delta S/S$) was calculated as $(S_C - S_L)/S_C$.

For DSC-CBF calculation, the transverse relaxation rate (ΔR_2^*) was calculated using the equation, $\Delta R_2^*(t) = -\ln\,(S(t)/S_0)/\text{TE}$, where $S(t)$ is the signal intensity at time t, S_0 is the average pre-Gd-DTPA baseline signal intensity, and TE is the echo time. Cerebral blood flow map was then generated by deconvolving the change in tissue concentration of

Gd-DTPA over the first pass with an arterial input function using singular value decomposition (Ostergaard *et al*, 1996*a*, *b*).

Comparison of CBF data between the two techniques used normalization with respect to the unaffected hemisphere to reduce intersubject variations, instead of using quantitative CBF values. In the stroke group, ASL-CBF map obtained for each PLD was normalized with respect to the average CBF value of pixels in the middle cerebral artery territory of unaffected left hemisphere (normal pixels) obtained with the PLD of 100 milliseconds. Dynamic susceptibility contrast CBF maps were also normalized by the mean DSC-CBF value of the pixels in the same area. In the hypercapnia group, mean CBF of the pixels in the middle cerebral artery area of the left hemisphere under air breathing status was used as a reference for each rat.

Hyperperfusion pixels in the stroke group were defined as pixels that had both ASL-CBF and DSC-CBF values greater than mean + 2 s.d. of normal pixels. The ASL:DSC ratio map was obtained by dividing the normalized ASL-CBF by the normalized DSC-CBF. T_1 ratio map was generated by dividing the T_1 map obtained before the injection of Gd-DTPA to the T_1 map obtained post-Gd-DTPA. Regions of increased permeability were defined as regions that showed T_1 ratio increase greater than (mean + 2 s.d.) of the normal region, indicating a leakage of Gd-DTPA.

Results

Blood pressures were not statistically different among groups and between before and after mannitol injection (stroke group: 117 ± 8 mm Hg; hypercapnia group: air breathing 125 ± 8 mm Hg, 5% CO_2 inhalation 116 ± 9 mm Hg; mannitol group: before injection 115 ± 12 mm Hg, after injection 133 ± 15 mm Hg), except for the transient increase immediately after mannitol injection. Normalization with contralateral middle cerebral artery territory was used to minimize residual systemic effects of mannitol.

Average CBF values of normal pixels by ASL and DSC were, respectively (1) 84 ± 3 and 93 ± 10 mL/100 g per minute (mean ± s.d., $n = 6$) in the stroke group, (2) 76 ± 14 and 106 ± 13 mL/100 g per minute ($n = 3$) in the hypercapnia group, and (3) 93 ± 9 and 109 ± 10 mL/100 g per minute ($n = 3$) in the mannitol group. There were statistically significant differences between ASL and DSC values (paired *t*-test), a result of systematic errors between the two methods. The ASL data are consistent with those reported previously in our laboratory under essentially identical conditions (Liu *et al*, 2004; Shen *et al*, 2003, 2004, 2005; Sicard *et al*, 2003; Sicard and Duong, 2005).

The mean T_1 values from regions of interest of the cerebral cortex, caudoputamen, corpus callosum, infarct core, and hyperperfusion pixels from the stroke group were 1.76 ± 0.14, 1.74 ± 0.09, 1.35 ± 0.11, 2.27 ± 0.29, and 1.93 ± 0.17 (mean ± s.d., $n = 6$), respectively. T_1 values of the infarct core and hyperperfusion pixels were statistically different from that of the cortex ($P < 0.05$). T_1 differences were taken into account in calculating ASL-CBF. The hypercapnia group showed no significant changes in T_1 value, indicating the absence of Gd-DTPA leakage. The mannitol group showed significant T_1 decrease indicating Gd-DTPA leakage (before mannitol 1.76 ± 0.14, after mannitol 1.51 ± 0.24).

Arterial Spin Labeling Versus Dynamic Susceptibility Contrast Cerebral Blood Flow

Figure 2A shows representative ASL-CBF, DSC-CBF, and ASL:DSC ratio maps from each of the three groups. In the stroke group, both ASL- and DSC-CBF maps showed hyperperfusion in the lesion hemisphere. The ASL:DSC CBF ratio was higher in the hyperperfusion pixels than the contralateral normal hemisphere. In the hypercapnia group, both the ASL- and DSC-CBF maps showed CBF increases in both hemispheres but the ASL:DSC CBF ratio map did not increase relative to baseline. In the mannitol group, both ASL- and DSC-CBF maps showed CBF increase predominantly in the hemisphere to which mannitol was injected. Similar to the stroke group, the mannitol group also showed a higher ASL-CBF compared with DSC-CBF, resulting in increased ASL:DSC CBF ratio.

Figure 2B shows the scatterplots of normalized ASL-CBF versus DSC-CBF group for a PLD of 100 milliseconds for each of the three groups. In the normal hemisphere or conditions, regression analysis showed strong correlations and slopes close to unity for all three groups (stroke group: $y = 0.96x$, $R^2 = 0.44$; hypercapnia group: $y = 0.97x$, $R^2 = 0.37$; and mannitol group: $y = 0.96x$, $R^2 = 0.38$). In contrast, the stroke and the mannitol-injected hemisphere showed greater-than-unity slopes (lesion hemisphere: $y = 1.21x$, $R^2 = 0.57\%$, 26% increase; mannitol-affected hemisphere: $y = 1.46x$, $R^2 = 0.43\%$, 52% increase), whereas the hypercapnia group showed a less-than-unity slope ($y = 0.86x$, $R^2 = 0.42\%$, 11% decrease).

Cerebral Blood Flow Values and Gd-DTPA Leakage in Postischemic Hyperperfusion

Figure 3A shows the T_1 maps before and after Gd-DTPA injection, the subtraction image ($T_{1\text{post-Gd}} - T_{1\text{pre-Gd}}$), and the ASL-CBF map of a representative rat from the stroke group. Hyperintensity on the subtraction image corresponded to the area with Gd-DTPA leakage and matched well with the area of higher ASL-CBF. Scatterplots between the normalized ASL-CBF (PLD = 100 milliseconds) and DSC-CBF from all rats in the stroke group 48 hours after cerebral ischemia are shown in Figure 3B. The majority (748/962 pixels, 78%) of the hyperperfusion pixels showed increased T_1 ratio (blue dots). Moreover, the hyperperfusion pixels had higher ASL-CBF than DSC-CBF. Figure 3C shows the group-averaged ASL:DSC CBF ratio from normal and hyperperfusion

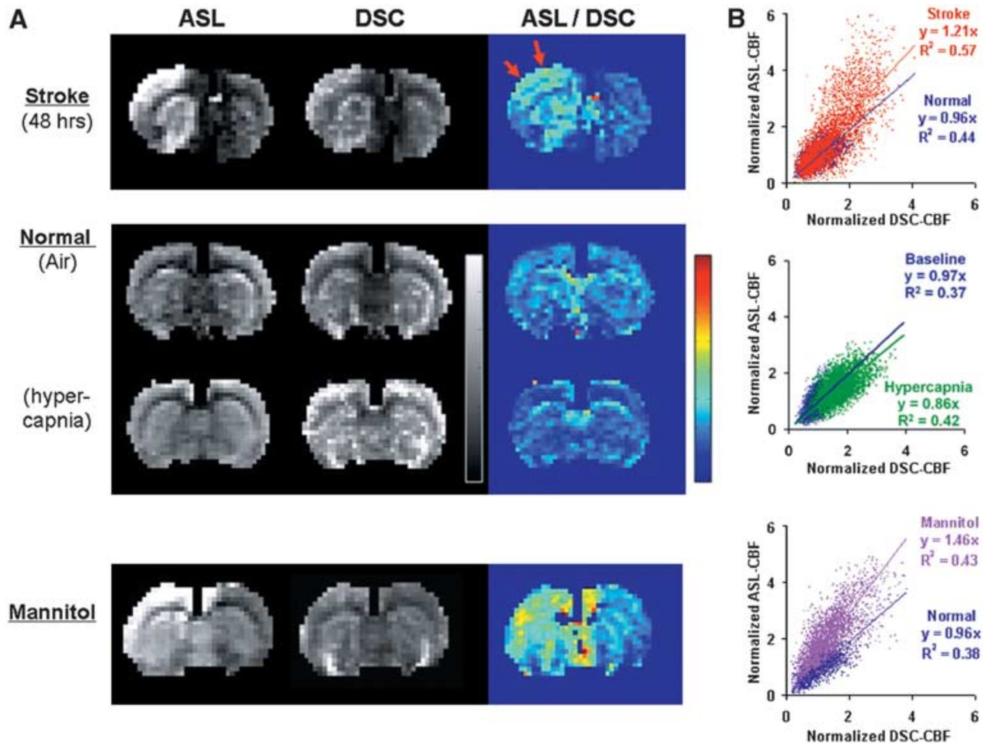

Figure 2 (**A**) Arterial spin labeling (ASL) cerebral blood flow (CBF) image, dynamic susceptibility contrast (DSC) CBF image, and ASL:DSC ratio maps from one animal of each of the three experimental groups. In the stroke animal (top row), the stroke lesion shows hyperperfusion. ASL yields a higher CBF than DSC. In the hypercapnia animal (middle row), CBF increases globally. ASL- and DSC-CBF maps show similar increases. In normal animal injected with mannitol (bottom row), CBF increases in the affected hemisphere. ASL yields a higher CBF increase than DSC. (**B**) Normalized ASL versus DSC CBF scatterplots for all animals in each of the three experimental groups. The slopes of the normal hemispheres in all three groups were close to unity. The slopes of the stroke, hypercapnia, and mannitol group were 1.21, 0.86, and 1.46, respectively.

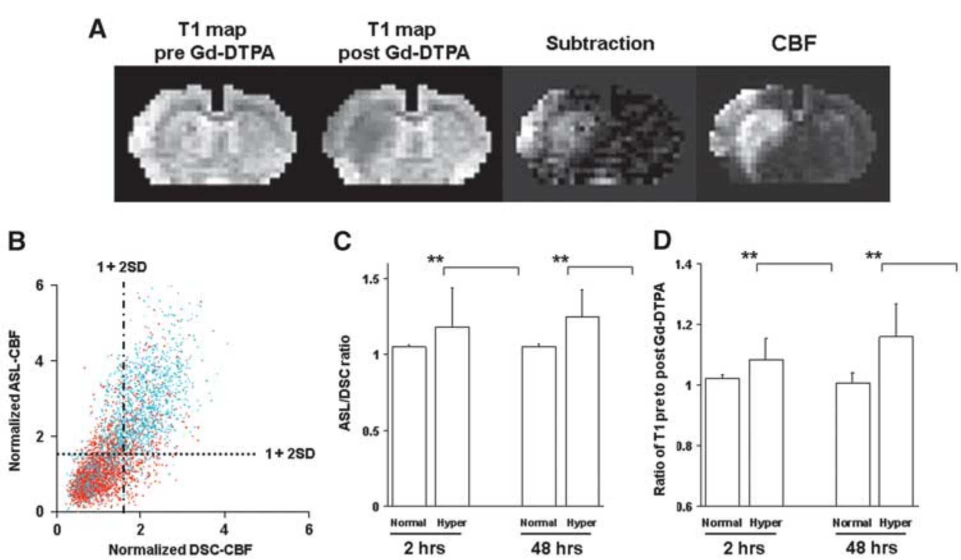

Figure 3 (**A**) T_1 maps before and after Gd-DTPA intravenous injection, subtraction image, and arterial spin labeling cerebral blood flow (ASL-CBF) map of a representative stroke rat. Hyperintensity on the subtraction image indicates Gd-DTPA leakage, which corresponds well to the area of increased CBF. (**B**) Normalized ASL (postlabeling delay (PLD) = 100) versus dynamic susceptibility contrast (DSC) CBF scatterplots of stroke group obtained at 48 hours after stroke. Pixels with ratio of T_1 pre- to post-Gd-DTPA greater than mean $T_1 + 2$ s.d. of contralateral normal pixels are displayed as blue dots. Normal T_1 pixels of the stroke hemisphere are shown as red dots. (**C**) Group-averaged ASL:DSC CBF ratios of the normal and the hyperperfusion pixels at 2 and 48 hours after stroke onset (PLD = 100). The ratio was larger in the hyperperfusion territory. (**D**) Group-averaged ratios of T_1 before and after Gd-DTPA from the normal and the hyperperfusion pixels at 2 and 48 hours after stroke. The ratio was also larger in the hyperperfusion territory.

pixels from the stroke group obtained at 2 and 48 hours after stroke (PLD = 100 milliseconds). The ASL:DSC CBF ratio increased significantly in the hyperperfusion area than that in the normal hemisphere at each time points. Similar conclusion was reached for the T_1 ratio data as depicted in Figure 3D.

To avoid Gd-DTPA effect of the first DSC measurement, the second ASL measurement was made 2 hours after the first. Arterial spin labeling was measured and confirmed $\Delta S/S$ fully recovered to baseline 90 minutes after Gd-DTPA injection in each rat.

ΔR_2^* Time Courses of Dynamic Susceptibility Contrast Magnetic Resonance Imaging

Figure 4 shows representative normalized ΔR_2^* time courses. ΔR_2^* trace of the normal pixels returned close to baseline after Gd-DTPA injection (i.e., time points > 25 seconds, normalized ΔR_2^* between 25 and 30 seconds = 0.06 ± 0.003). Similarly, pixels from the hypercapnia group also showed the ΔR_2^* trace returned close to baseline after Gd-DTPA injection (normalized ΔR_2^* between 25 and 30 seconds = 0.07 ± 0.005). In marked contrast, ΔR_2^* trace of the hyperperfusion pixels in the stroke group remained significantly elevated from the baseline by comparison (normalized ΔR_2^* between 25 and 30 seconds = 0.16 ± 0.008). In the mannitol group, ΔR_2^* trace of the pixels with T_1:T_1 with Gd-DTPA ratio larger than mean + 2 s.d. of normal values were slightly elevated compared with normal (normalized ΔR_2^* between 25 and 30 seconds = 0.09 ± 0.006). The timing of the first passes of the three groups differed, with the hyperperfusion pixels in the stroke group showed the most delayed first pass.

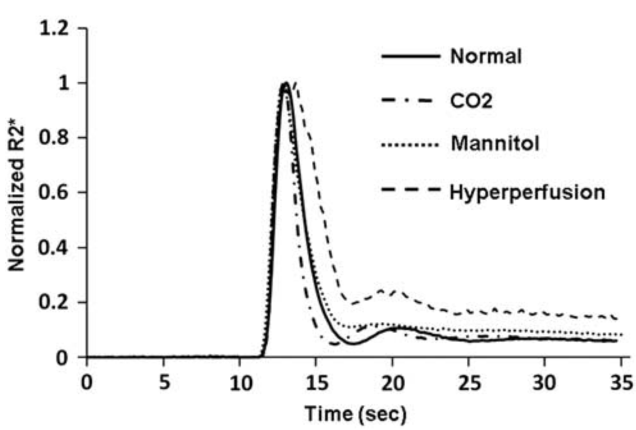

Figure 4 Normalized ΔR_2^* time courses for three experimental groups. The traces from the normal and hypercapnia group returned close to baseline after bolus gadopentetate dimeglumine (Gd-DTPA) injection. The mannitol group shows a slight elevation post-Gd-DTPA. In contrast, trace from the hyperperfusion pixels remains significantly elevated above baseline.

Arterial Spin Labeling Cerebral Blood Flow Versus Arterial Transit Time in Postischemic Hyperperfusion

Figure 5A shows the representative MRA of a stroke rat imaged at different time points. The MRA acquired at 2 hours after recombinant tissue plasminogen activator injection revealed recanalization of the right middle cerebral artery (arrows). The MRA at 48 hours after stroke also showed many dilated vessels in the affected hemisphere (arrow heads). The ASL:DSC CBF ratio from hyperperfusion and normal pixels were analyzed for multiple PLDs (Figure 5B). The ASL:DSC CBF ratio decreased significantly with increasing PLD in both normal and hyperperfusion pixels. However, the ratio of the hyperperfusion pixels dropped to a larger extent than that of the normal pixels ($P < 0.05$). The relationship between $\Delta S/S$ and PLD of the normal pixels and the hyperperfusion pixels is depicted in Figure 5C. The $\Delta S/S$ reached a maximum at PLD of 200 milliseconds in hyperperfusion pixels and 300 milliseconds in normal pixels.

Discussion

This study examined how changes in tissue spin-lattice relaxation-time constant, BBB permeability, and arterial transit time affect CBF quantification by ASL and DSC in postischemic hyperperfusion in same rats. Embolic stroke rats imaged 48 hours after reperfusion showed reliable regional hyperperfusion. Arterial spin labeling and DSC-CBF of normal pixels linearly correlated, whereas ASL-CBF of hyperperfusion pixels were higher than DSC-CBF. T_1 of hyperperfusion pixels were higher, transit time was shortened, and ΔR_2^* time courses showed Gd-DTPA leakages in hyperperfusion regions. Hypercapnic inhalation, which does not change BBB permeability, showed overall CBF increase but ASL- and DSC-CBF remain linearly correlated. Mannitol injection, which increases BBB permeability, showed ASL-CBF to be higher than DSC-CBF. We concluded that (1) under normal conditions the commonly used ASL and DSC provide comparable quantitative CBF values and (2) in ischemic hyperperfusion, T_1 and BBB disruption were responsible for discrepancy in CBF measured by ASL and DSC. These findings could have important implications in stroke MRI.

Effect of Permeability Change to Arterial Spin Labeling and Dynamic Susceptibility Contrast Measurements

Arterial spin labeling and DSC-CBF values were comparable in normal brain, in good agreement with previous reports (Lia *et al*, 2000; Weber *et al*, 2003). The ASL-CBF and DSC-CBF were higher in the hyperperfusion pixels in all three experimental groups. The ASL/DSC ratios of the hyperperfusion pixels were higher in the stroke group and mannitol group, but not in the hypercapnia group. The majority of hyperperfusion pixels in the stroke group showed

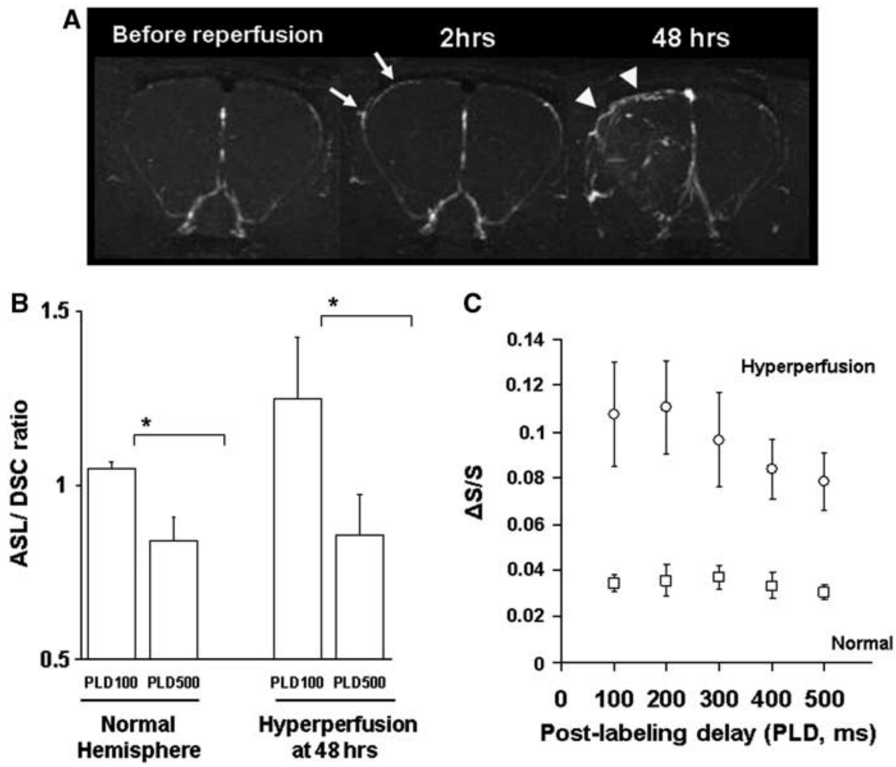

Figure 5 (**A**) Magnetic resonance angiography (MRA) of a stroke rat imaged before, 2 and 48 hours after recanalization. Recanalization was detected at 2 hours (arrows). Additional vessels were highly perfused at 48 hours (arrow heads). (**B**) Group-averaged arterial spin labeling to dynamic susceptibility contrast (ASL:DSC) cerebral blood flow (CBF) ratio of the hyperperfusion pixels and contralateral normal pixels of middle cerebral artery area at postlabeling delays (PLDs) of 100 and 500 milliseconds. ASL:DSC ratio decreases with increasing PLD. (**C**) $\Delta S/S$ versus PLD in the normal and hyperperfusion area. The $\Delta S/S$ of the hyperperfusion pixels peaked at PLD of 200 milliseconds and the $\Delta S/S$ of normal pixels peaked at PLD of 300 milliseconds. $*P < 0.05$.

Gd-DTPA leakage, whereas those in the hypercapnia group did not show significant T_1 change. A possible explanation of these observations is that BBB permeability differed among these groups. Water is not freely diffusible across the BBB (Herscovitch *et al*, 1987; Schwarzbauer *et al*, 1997; Silva *et al*, 1997). However, most published ASL-CBF calculations (including this study) assumed labeled water in the blood is freely diffusible endogenous tracer (Detre *et al*, 1992; Kim, 1995; Kwong *et al*, 1992). In postischemic hyperperfusion, BBB is disrupted by ischemia and water in the blood can extravasate more freely, resulting in CBF overestimation by the ASL approach herein. By contrast, CBF is likely underestimated in hypercapnia group because the water extraction fraction decreases with increased CBF in intact BBB (Silva *et al*, 1997).

Similarly, DSC MRI is also confounded by the compromised BBB in hyperperfusion regions. Leaked Gd-DTPA could shorten both T_1 and T_2^* values of tissue. Whether DSC-CBF is underestimated or overestimated depends on whether T_1 or T_2^* effects by leaked Gd-DTPA dominated. T_1 increase of accumulated Gd-DTPA in the interstitial space overwhelmed T_2^* decrease when short TR spin echo echo-planar imaging was used (Lim *et al*, 2003). Our results showed that ΔR_2^* of most of the hyperperfusion pixels remained higher than that in normal tissue after bolus passage, suggesting that T_2^* effect was dominant. Although T_1 shortening effect could be minimized by using a double-echo technique (Heiland *et al*, 1999; Uematsu *et al*, 2000), T_2^* effect by leaked Gd-DTPA cannot be distinguished from DSC-CBF effect.

It is interesting to note that some hyperperfusion pixels did not show significant Gd-DTPA leakage. It may be because of the difference between the permeability of water and Gd-DTPA. It may also be because of the sensitivity of T_1 measurement *per se* and measuring the time course of the leakage may be more sensitive (Ewing *et al*, 2003; Jiang *et al*, 2005; Tofts and Kermode, 1991).

Effect of T_1 and Arterial Transit Time Change on Arterial Spin Labeling and Dynamic Susceptibility Contrast Measurement

T_1 value of hyperperfusion region was 1.93 seconds, compared with that of normal cortex of 1.76 seconds. The T_1 increase resulted in 8% decrease in ASL-CBF value. Although DSC-CBF quantification is not significantly affected by T_1 difference in a typical measurement, tissue T_2^* changes due to Gd-DTPA leakage contributed to CBF accuracy (Ostergaard *et al*, 1996*b*).

In the hyperperfusion area, the arterial transit time was reduced. Thus, CBF accuracy with a PLD typically used for normal brain was not an issue for the hyperperfusion pixel. Although it was not investigated herein, ASL- and DSC-CBF accuracies are also affected in region of perfusion deficit associated with stroke. Thomas *et al* (2006) reported that longer PLD (e.g., 800 to 1,000 milliseconds) is required for spin echo CASL sequence to maintain CBF analysis insensitive to transit time because of the transit time delay. Delayed arterial transit time also affects DSC-CBF quantification, especially in ischemic hypoperfused area, resulting in underestimation of CBF (Calamante *et al*, 2000; Ostergaard *et al*, 1996*b*). Fourier-based or delay invariant block-circulant singular value decomposition methods have been proposed to minimize this effect (Ostergaard *et al*, 1996*b*; Smith *et al*, 2000; Wu *et al*, 2003*b*). Another problem for DSC-CBF quantification is dispersion (Calamante *et al*, 2000). Increasing dispersion underestimates DSC-CBF because DSC model cannot distinguish feeding vessels dispersion from tissue microvasculature dispersion. Our data show that DSC-CBF values in each group were affected by dispersion differently. Although correction for dispersion has been proposed (Ostergaard *et al*, 1999; Willats *et al*, 2008), dispersion correction is less straightforward.

Conclusion

Under normal conditions, the commonly used ASL and DSC approach provide comparable quantitative values. In ischemic hyperperfusion, changes in T_1 and BBB disruption that result in increased water permeability and Gd-DTPA leakage are likely responsible for discrepancy between CBF measured by ASL and DSC technique. The ASL model overestimates CBF due to increased permeability in postischemic hyperperfusion and DSC overestimates CBF due to ΔR_2^* effects from Gd-DTPA leakage. Arterial spin labeling CBF is higher than DSC-CBF by $\sim$25% in the hyperperfusion pixels. Caution must be exercised when using various CBF methods in stroke imaging. Future studies will incorporate T_1, arterial transit time, and permeability into the ASL and DSC analysis, and compare with positron emission tomography in the same animals.

Disclosure/conflict of interest

The authors declare no conflict of interest.

References

Alsop DC, Detre JA (1996) Reduced transit-time sensitivity in noninvasive magnetic resonance imaging of human cerebral blood flow. *J Cereb Blood Flow Metab* 16:1236–49

Calamante F, Gadian DG, Connelly A (2000) Delay and dispersion effects in dynamic susceptibility contrast MRI: simulations using singular value decomposition. *Magn Reson Med* 44:466–73

Chalela JA, Alsop DC, Gonzalez-Atavales JB, Maldjian JA, Kasner SE, Detre JA (2000) Magnetic resonance perfusion imaging in acute ischemic stroke using continuous arterial spin labeling. *Stroke* 31:680–7

Detre JA, Leigh JS, Williams DS, Koretsky AP (1992) Perfusion imaging. *Magn Reson Med* 23:37–45

Donahue KM, Krouwer HG, Rand SD, Pathak AP, Marszalkowski CS, Censky SC, Prost RW (2000) Utility of simultaneously acquired gradient-echo and spin-echo cerebral blood volume and morphology maps in brain tumor patients. *Magn Reson Med* 43:845–53

Duong TQ, Silva AC, Lee SP, Kim SG (2000) Functional MRI of calcium-dependent synaptic activity: cross correlation with CBF and BOLD measurements. *Magn Reson Med* 43:383–92

Ewing JR, Knight RA, Nagaraja TN, Yee JS, Nagesh V, Whitton PA, Li L, Fenstermacher JD (2003) Patlak plots of Gd-DTPA MRI data yield blood-brain transfer constants concordant with those of 14C-sucrose in areas of blood-brain opening. *Magn Reson Med* 50:283–92

Heiland S, Benner T, Debus J, Rempp K, Reith W, Sartor K (1999) Simultaneous assessment of cerebral hemodynamics and contrast agent uptake in lesions with disrupted blood-brain-barrier. *Magn Reson Imaging* 17:21–7

Herscovitch P, Raichle ME (1985) What is the correct value for the brain–blood partition coefficient for water? *J Cereb Blood Flow Metab* 5:65–9

Herscovitch P, Raichle ME, Kilbourn MR, Welch MJ (1987) Positron emission tomographic measurement of cerebral blood flow and permeability-surface area product of water using [15O]water and [11C]butanol. *J Cereb Blood Flow Metab* 7:527–42

Jiang Q, Ewing JR, Ding GL, Zhang L, Zhang ZG, Li L, Whitton P, Lu M, Hu J, Li QJ, Knight RA, Chopp M (2005) Quantitative evaluation of BBB permeability after embolic stroke in rat using MRI. *J Cereb Blood Flow Metab* 25:583–92

Kim SG (1995) Quantification of relative cerebral blood flow change by flow-sensitive alternating inversion recovery (FAIR) technique: application to functional mapping. *Magn Reson Med* 34:293–301

Kwong KK, Belliveau JW, Chesler DA, Goldberg IE, Weisskoff RM, Poncelet BP, Kennedy DN, Hoppel BE, Cohen MS, Turner R *et al* (1992) Dynamic magnetic resonance imaging of human brain activity during primary sensory stimulation. *Proc Natl Acad Sci USA* 89:5675–9

Lia TQ, Guang Chen Z, Ostergaard L, Hindmarsh T, Moseley ME (2000) Quantification of cerebral blood flow by bolus tracking and artery spin tagging methods. *Mag Reson Imaging* 18:503–12

Lim CC, Roberts TP, Sitoh YY, Hui F (2003) Rising signal intensity observed in extra-axial brain tumours—a potential pitfall in perfusion MR imaging. *Singapore Med J* 44:526–30

Liu ZM, Schmidt KF, Sicard KM, Duong TQ (2004) Imaging oxygen consumption in forepaw somatosensory stimulation in rats under isoflurane anesthesia. *Magn Reson Med* 52:277–85

Macfarlane R, Moskowitz MA, Sakas DE, Tasdemiroglu E, Wei EP, Kontos HA (1991) The role of neuroeffector mechanisms in cerebral hyperperfusion syndromes. *J Neurosurg* 75:845–55

Marchal G, Young AR, Baron JC (1999) Early postischemic hyperperfusion: pathophysiologic insights from positron emission tomography. *J Cereb Blood Flow Metab* 19:467–82

Ostergaard L, Chesler DA, Weisskoff RM, Sorensen AG, Rosen BR (1999) Modeling cerebral blood flow and flow heterogeneity from magnetic resonance residue data. *J Cereb Blood Flow Metab* 19:690–9

Ostergaard L, Sorensen AG, Kwong KK, Weisskoff RM, Gyldensted C, Rosen BR (1996*a*) High resolution measurement of cerebral blood flow using intravascular tracer bolus passages. Part II: Experimental comparison and preliminary results. *Magn Reson Med* 36:726–36

Ostergaard L, Weisskoff RM, Chesler DA, Gyldensted C, Rosen BR (1996*b*) High resolution measurement of cerebral blood flow using intravascular tracer bolus passages. Part I: mathematical approach and statistical analysis. *Magn Reson Med* 36:715–25

Pan J, Konstas AA, Bateman B, Ortolano GA, Pile-Spellman J (2007) Reperfusion injury following cerebral ischemia: pathophysiology, MR imaging, and potential therapies. *Neuroradiology* 49:93–102

Parkes LM, Tofts PS (2002) Improved accuracy of human cerebral blood perfusion measurements using arterial spin labeling: accounting for capillary water permeability. *Magn Reson Med* 48:27–41

Rapoport SI (2000) Osmotic opening of the blood–brain barrier: principles, mechanism, and therapeutic applications. *Cell Mol Neurobiol* 20:217–30

Schaller B, Graf R (2004) Cerebral ischemia and reperfusion: the pathophysiologic concept as a basis for clinical therapy. *J Cereb Blood Flow Metab* 24:351–71

Schwarzbauer C, Morrissey SP, Deichmann R, Hillenbrand C, Syha J, Adolf H, Noth U, Haase A (1997) Quantitative magnetic resonance imaging of capillary water permeability and regional blood volume with an intravascular MR contrast agent. *Magn Reson Med* 37:769–77

Shen Q, Fisher M, Sotak CH, Duong TQ (2004) Effects of reperfusion on ADC and CBF pixel-by-pixel dynamics in stroke: characterizing tissue fates using quantitative diffusion and perfusion imaging. *J Cereb Blood Flow Metab* 24:280–90

Shen Q, Meng X, Fisher M, Sotak CH, Duong TQ (2003) Pixel-by-pixel spatiotemporal progression of focal ischemia derived using quantitative perfusion and diffusion imaging. *J Cereb Blood Flow Metab* 23:1479–88

Shen Q, Ren H, Cheng H, Fisher M, Duong TQ (2005) Functional, perfusion and diffusion MRI of acute focal ischemic brain injury. *J Cereb Blood Flow Metab* 25:1265–79

Sicard K, Shen Q, Brevard ME, Sullivan R, Ferris CF, King JA, Duong TQ (2003) Regional cerebral blood flow and BOLD responses in conscious and anesthetized rats under basal and hypercapnic conditions: implications for functional MRI studies. *J Cereb Blood Flow Metab* 23:472–81

Sicard KM, Duong TQ (2005) Effects of hypoxia, hyperoxia and hypercapnia on baseline and stimulus-evoked BOLD, CBF and CMRO2 in spontaneously breathing animals. *Neuroimage* 25:850–8

Silva AC, Zhang W, Williams DS, Koretsky AP (1997) Estimation of water extraction fractions in rat brain using magnetic resonance measurement of perfusion with arterial spin labeling. *Magn Reson Med* 37:58–68

Smith AM, Grandin CB, Duprez T, Mataigne F, Cosnard G (2000) Whole brain quantitative CBF and CBV measurements using MRI bolus tracking: comparison of methodologies. *Magn Reson Med* 43:559–64

Tanaka Y, Ishii H, Hiraoka M, Miyasaka N, Kuroiwa T, Hajjar KA, Nagaoka T, Duong TQ, Ohno K, Yoshida M (2007) Efficacy of recombinant annexin 2 for fibrinolytic therapy in a rat embolic stroke model: a magnetic resonance imaging study. *Brain Res* 1165:135–43

Thomas DL, Lythgoe MF, van der Weerd L, Ordidge RJ, Gadian DG (2006) Regional variation of cerebral blood flow and arterial transit time in the normal and hypoperfused rat brain measured using continuous arterial spin labeling MRI. *J Cereb Blood Flow Metab* 26:274–82

Tofts PS, Kermode AG (1991) Measurement of the blood–brain barrier permeability and leakage space using dynamic MR imaging. 1. Fundamental concepts. *Magn Reson Med* 17:357–67

Uematsu H, Maeda M, Sadato N, Matsuda T, Ishimori Y, Koshimoto Y, Yamada H, Kimura H, Kawamura Y, Matsuda T, Hayashi N, Yonekura Y, Ishii Y (2000) Vascular permeability: quantitative measurement with double-echo dynamic MR imaging—theory and clinical application. *Radiology* 214:912–7

Weber MA, Gunther M, Lichy MP, Delorme S, Bongers A, Thilmann C, Essig M, Zuna I, Schad LR, Debus J, Schlemmer HP (2003) Comparison of arterial spin-labeling techniques and dynamic susceptibility-weighted contrast-enhanced MRI in perfusion imaging of normal brain tissue. *Invest Radiol* 38:712–8

Willats L, Connelly A, Calamante F (2008) Minimising the effects of bolus dispersion in bolus-tracking MRI. *NMR Biomed* 21:1126–37

Williams DS, Detre JA, Leigh JS, Koretsky AP (1992) Magnetic resonance imaging of perfusion using spin inversion of arterial water. *Proc Natl Acad Sci USA* 89:212–6

Wu O, Ostergaard L, Koroshetz WJ, Schwamm LH, O'Donnell J, Schaefer PW, Rosen BR, Weisskoff RM, Sorensen AG (2003*a*) Effects of tracer arrival time on flow estimates in MR perfusion-weighted imaging. *Magn Reson Med* 50:856–64

Wu O, Ostergaard L, Weisskoff RM, Benner T, Rosen BR, Sorensen AG (2003*b*) Tracer arrival timing-insensitive technique for estimating flow in MR perfusion-weighted imaging using singular value decomposition with a block-circulant deconvolution matrix. *Magn Reson Med* 50:164–74

Zaharchuk G, Straka M, Marks MP, Albers GW, Moseley ME, Bammer R (2010) Combined arterial spin label and dynamic susceptibility contrast measurement of cerebral blood flow. *Magn Reson Med* 63:1548–56